Helical Polyacetylene Synthesized with a Chiral Nematic Reaction Field

K. Akagi,* G. Piao, S. Kaneko, K. Sakamaki,
H. Shirakawa,* M. Kyotani

Helical polyacetylene was synthesized under an asymmetric reaction field consisting of chiral nematic (N*) liquid crystals (LCs). The chiral nematic LC was prepared by adding a chiroptical binaphthol derivative as a chiral dopant to a mixture of two nematic LCs. Acetylene polymerizations were carried out using the catalyst titanium tetra-*n*-butoxide–triethylaluminum dissolved in the chiral nematic LC solvent. The polyacetylene film was shown by scanning electron microscopy to consist of clockwise or counterclockwise helical structure of fibrils. A Cotton effect was observed in the region of the $\pi \rightarrow \pi^*$ transition of the polyacetylene chain in circular dichroism spectra. The high electrical conductivities of ~1500 to 1800 siemens per centimeter after iodine doping and the chiral helicity of these films may be exploited in electromagnetic and optical applications.

Polyacetylene is the simplest linear conjugated macromolecule and a representative of conducting polymers (*1*). Pristine polyacetylene is a typical semiconductor, but its electrical conductivity can be varied by more than 14 orders of magnitude through doping. The maximum conductivity reported to date is more than 10^5 S/cm (*2, 3*). Although there is a divergent view by Božović, who proposed helical models (*4*), a planar structure has been generally accepted for both *cis*- and *trans*-polyacetylenes (*5*). If it were possible to modify such a planar structure of polyacetylene into a helical one, novel magnetic and optical properties might be expected. In earlier studies (*6–11*), we developed a polymerization method for highly aligned polyacetylene films by using nematic LC as a polymerization solvent for a homogeneous Ziegler-Natta catalyst composed of $Ti(O\text{-}n\text{-}Bu)_4$–$Et_3Al$ and achieved high electrical conductivities of 10^4 S/cm. Here, we report polymerization of acetylene under an asymmetric and anisotropic reaction field constructed with chiral nematic LCs and show that polyacetylene films formed by helical chains and fibrils can be synthesized.

(*R*)- and (*S*)-1,1′-bi-naphthyl-2,2′-bis[*para*-(*trans*-4-*n*-pentylcyclohexyl)phenoxy-1-hexyl]ether were synthesized through the Williamson etherification reactions of chiroptical (*R*)-(+)- and (*S*)-(−)-1,1′-bi-2-naphthols, respectively, with phenylcyclohexyl derivatives. The products will hereafter be abbreviated as (*R*)- and (*S*)-PCH506-binol (Scheme 1). Note that the substituent is composed of a phenylcyclohexyl (PCH) moiety, an *n*-pentyl group, and a hexamethylene chain linked to the PCH group via an ether-type oxygen atom, [-$(CH_2)_6$O-, 06], and is thus abbreviated as PCH506. Specific rotatory powers, $[\alpha]_D$, of the (*R*)- and (*S*)-binol derivatives were +24.0 and −10.0, respectively, in tetrahydrofuran at 24°C. The smaller absolute value of $[\alpha]_D$ for the (*S*)-binol derivative compared with that for the (*R*)-binol derivative should be ascribed to partial racemization during the etherification reaction (*12*). The (*S*)-binol derivative includes a certain amount of racemates, resulting in a lowering of optical purity. This is also confirmed by circular dichroism (CD) spectra of (*R*)- and (*S*)-binol derivatives (Fig. 1A).

To prepare an induced chiral nematic LC, we added 5 to 14 weight % of (*R*)- or (*S*)-PCH506-binol as a chiral dopant to the equal-weight mixture of the nematic LCs 4-(*trans*-4-*n*-propylcyclohexyl)ethoxybenzene (PCH302) and 4-(*trans*-4-*n*-propylcyclohexyl)butoxybenzene (PCH304). The PCH506 substituent group in the (*R*)- and (*S*)-PCH506-binol enhances the miscibility between the nematic LC mixture and the binol derivative used as the chiral dopant (Scheme 2). Use of a similar substituent with a shorter methylene spacer such as PCH503 or a normal alkyl substituent gave insufficient miscibility, yielding no chiral nematic phase. In polarizing optical micrographs of the mixture of PCH302, PCH304, and (*R*)-PCH506-binol (abbreviated as *R*-1) and that of PCH302, PCH304, and (*S*)-PCH506-binol (abbreviated as *S*-1), a striated fan-shaped texture and a striated Schlieren texture were observed in the (*R*-1) and (*S*-1) mixtures, respectively (Fig. 2). Both textures are characteristic of chiral nematic LC phases. The distance between the striae corresponds to a helical pitch, and thus, the (*S*-1) mixture has a longer helical pitch than the (*R*-1) mixture. In other words, the degree of helicity in the former is less than that of the latter. This can be rationalized by considering the smaller specific rotatory power of the (*S*)-PCH506-binol mentioned above. Nevertheless, measurements in a differential scanning calorimeter showed that both mixtures exhibit quite similar phase transition temperatures as well as enantiotropic behaviors (Scheme 2).

Cholesteryl chloride is known to be a clockwise chiral nematic (cholesteric) LC, and therefore is a feasible candidate for performing a miscibility test with our LCs. A mixture of (*R*-1)-LC and cholesteryl chloride lost the striae characteristic of a chiral nematic phase in the optical microscope, instead yielding features corresponding to an ordinary nematic phase. In contrast, the mixture of (*S*-1)-LC and cholesteryl chloride showed no change in optical texture, remaining in a chiral nematic phase. These results demonstrate that the screw directions of the (*R*)- and (*S*)-chiral nematic LCs are opposite to and the same as that of cholesteryl chloride, that is, they are counterclockwise and

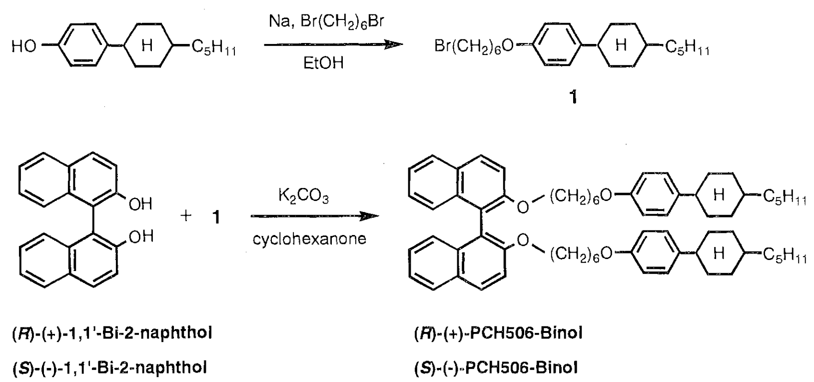

Scheme 1

K. Akagi, G. Piao, H. Shirakawa, Institute of Materials Science and Center of Tsukuba Advanced Research Alliance, University of Tsukuba, Tsukuba, Ibaraki 305-8573, Japan. S. Kaneko, K. Sakamaki, Institute of Materials Science, University of Tsukuba, Tsukuba, Ibaraki 305-8573, Japan. M. Kyotani, National Institute of Materials and Chemical Research, Tsukuba, Ibaraki 305-0046, Japan, and Center of Tsukuba Advanced Research Alliance, University of Tsukuba, Tsukuba, Ibaraki 305-8577, Japan.

*To whom correspondence should be addressed. E-mail: akagi@ims.tsukuba.ac.jp (K.A.) and hideki@ims.tsukuba.ac.jp (H.S.)

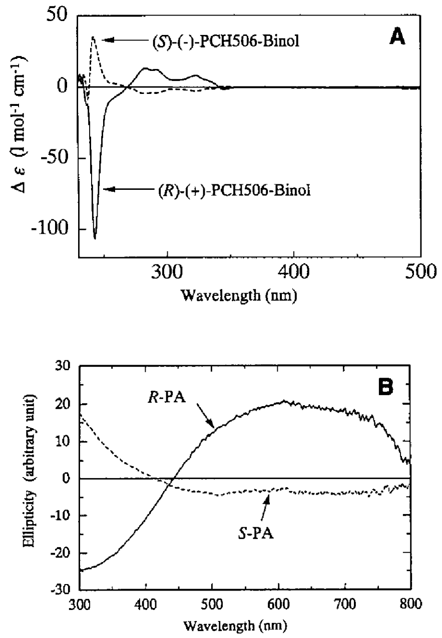

Fig. 1. (**A**) CD spectra of chiral dopants and (**B**) helical polyacetylene films. (A) (*R*)-(+)- and (*S*)-(−)-PCH506-binols. $\Delta\varepsilon$ (= $\varepsilon_L - \varepsilon_R$) is the difference of molar extinction coefficients (ε_L, ε_R) of sample to left and right circular polarized lights, and it is also correlated with molecular ellipticity [θ], that is, $[\theta] \approx 3300 \times \Delta\varepsilon$. (B) *R*-PA and *S*-PA indicate polyacetylene films synthesized under (*R*)- and (*S*)-chiral nematic liquid crystals, respectively.

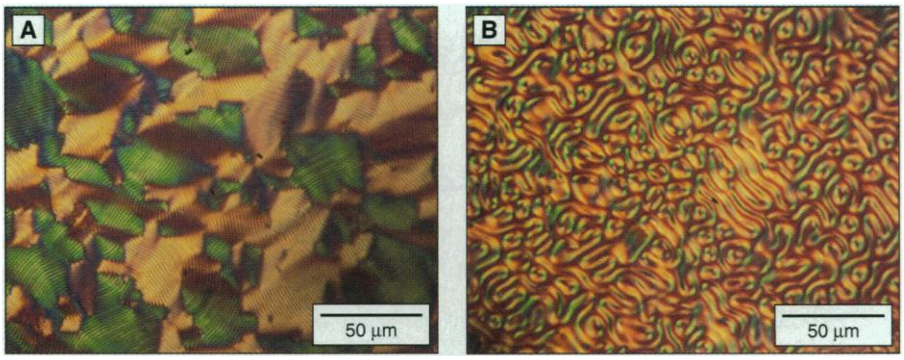

Fig. 2. Polarizing optical micrographs of the mixtures of PCH302, PCH304, and (*R*)- or (*S*)-PCH506-binol. (**A**) (*R*-1); PCH302:PCH304:(*R*)-PCH506-binol = 100:100:5 (weight %) at 31°C. (**B**) (*S*-1); PCH302:PCH304:(*S*)-PCH506-binol = 100:100:5 (weight %) at 17°C.

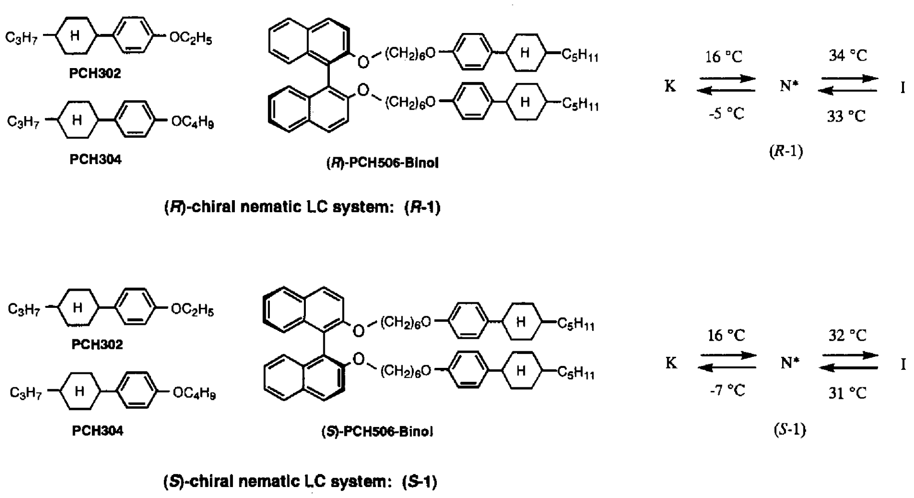

Scheme 2

clockwise, respectively.

Next, the (*R*)- and (*S*)-chiral nematic LCs were used as solvents for the Ziegler-Natta catalyst consisting of Ti(O-*n*-Bu)$_4$ and Et$_3$Al. The concentration of Ti(O-*n*-Bu)$_4$ was 15 mmol/l, and the mole ratio of the cocatalyst to catalyst, [Et$_3$Al]/[Ti(O-*n*-Bu)$_4$], was 4.0. The catalyst solution was aged for 0.5 hours at room temperature. During aging, the chiral nematic LCs containing the catalyst showed no noticeable change in their optical texture from that shown in Fig. 2, and only a slight lowering of the transition temperature by 2° to 5°C; the transition temperature between the solid and chiral nematic phases was 16° to 17°C, and that between the chiral nematic and isotropic ones was 30° to 31°C. No solidification was observed down to −7°C as a result of supercooling. Thus, the (*R*)- and (*S*)-chiral nematic LCs are confirmed to be chemically stable to the catalyst. Therefore, we were able to employ these LCs as asymmetric and anisotropic solvents for acetylene polymerization.

Acetylene gas of six-nines grade (99.9999%) purity was used without further purification. The apparatus and procedure employed were similar to those in earlier studies (*8, 9*), except for the polymerization temperature. Here, the polymerization temperature was kept between 17° and 18°C to maintain the chiral nematic phase, by circulating cooled ethanol through an outer flask enveloping the Schlenk flask. The initial acetylene pressure was 11.6 to 22.6 torr, and the polymerization time was 10 to 43 min. After polymerization, polyacetylene films were carefully stripped off the container and washed with toluene several times under argon gas at room temperature. The films were dried through vacuum pumping on a Teflon sheet and stored in a freezer at −20°C.

Scanning electron microscope (SEM) images of polyacetylene films show that the polyacetylenes synthesized under the (*R*)- and (*S*)-chiral nematic LCs form helical fibrillar morphologies with counterclockwise and clockwise directions, respectively (Figs. 3 and 4). The screw directions of the fibrils are the same as those of the chiral nematic LCs used as solvents. The helical polyacetylene thus seems to replicate the helical structure of the chiral nematic LCs employed as an asymmetric reaction field. In CD spectra of the polyacetylene thin films synthesized under the (*R*)- and (*S*)-chiral nematic LCs, positive and negative Cotton effects, respectively, were observed in the region from 450 to 800 nm wavelength (Fig. 1B), corresponding to the π → π* transition of the polyacetylene chain, despite the absence of chiroptical substituents in side chains. This indicates that the polyacetylene chain itself is helically screwed. It is evident that the aforementioned Cotton effect is not due to the chiral dopant [(*R*)- or (*S*)-PCH506-binols], because the Cotton effect of the chiral dopant is only observed at the shorter wavelengths of 240 to 340 nm (Fig. 1A). It should be noted that the negative Cotton effect of the clockwise *S*-polyacetylene is smaller than the positive one of the counterclockwise *R*-polyacetylene (Fig. 1B). This means that the degree of helicity in the *S*-polyacetylene chain is less than that of the *R*-one, as a result of the smaller specific rotatory power of the (*S*)-PCH506-binol. The difference

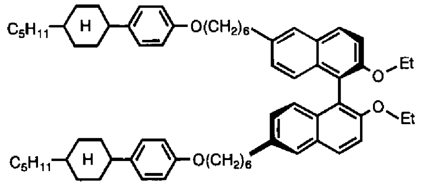

Scheme 3

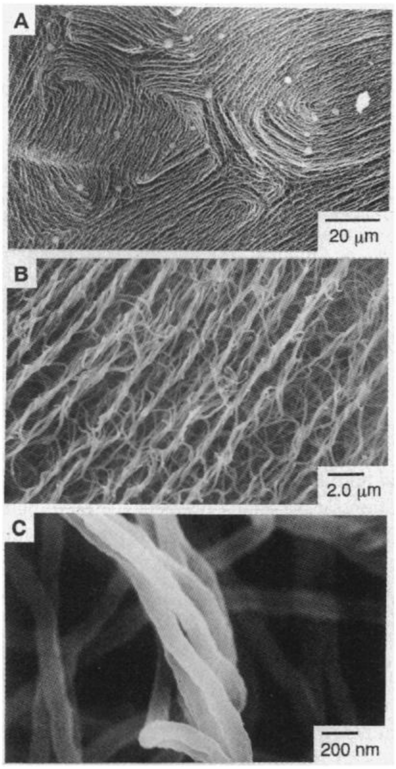

Fig. 3. SEM micrographs of polyacetylene film synthesized with (*R*)-chiral nematic liquid crystal at increasing magnification.

in the specific rotatory power between the (*R*)- and (*S*)-PCH506-binol is also reflected in the SEM micrographs of the helical structures of fibrils (Figs. 3 and 4).

From these results, we conclude that counterclockwise and clockwise helical polyacetylene chains are formed under (*R*)- and (*S*)-chiral nematic LCs, respectively, and that these helical chains are further bundled through van der Waals interactions to form helical fibrils with the same screw directions as those of the chiral nematic LCs. The helical pitch of the chiral nematic LC depends on the optical purity of the chiral dopant, as exemplified in the (*R*)- and (*S*)-PCH506-binols. This implies that the helical pitch of the polyacetylene chain can be varied by changing the optical purity of the chiral dopant. Another axially chiral dopant, (*R*)-(+)-6,6′-bis-PCH506-2,2′-di-Et-binol (Scheme 3) (*13*) gave a shorter helical pitch of chiral nematic LC by 0.3 μm than that of (*R*)-PCH506-binol. Acetylene polymerization with this chiral nematic LC afforded clearer helical morphologies in SEM micrographs (Fig. 5), resulting in hierarchical higher-order structures (*14*). The bundles of fibrils are screwed counterclockwise (Fig. 5C), with the same screw direction as that of the chiral nematic LC. These bundles are aligned parallel to each other in the microscopic regime (Fig. 5B) and form spiral morphologies in the macroscopic regime (Fig. 5A).

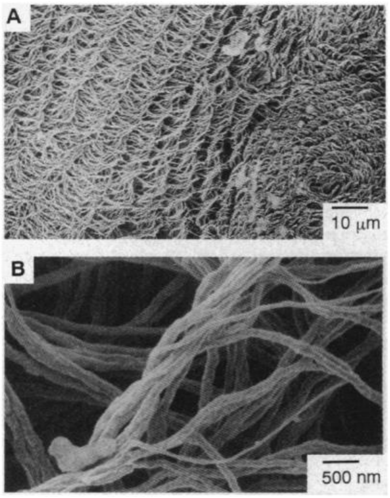

Fig. 4. SEM micrographs of polyacetylene film synthesized with (*S*)-chiral nematic liquid crystal at two different magnifications.

To evaluate the helicity of this polyacetylene, we estimated the dihedral angle between neighboring unit cells (–CH=CH–) and found that the value ranged from 0.02° to 0.23°. Although such a very small dihedral angle may allow us to regard this polyacetylene as an approximately planar structure, the polymers are rigorously screwed in the direction of the non-zero dihedral angle. These helical polyacetylene films have high *trans* contents of 90% and become highly conductive upon iodine doping. In fact, the electrical conductivities of the doped films are ~1.5×10^3 to 1.8×10^3 S/cm at room temperature, comparable to those of metals. Iodine-doped polyacetylene showed the same Cotton effect as that of nondoped polyacetylene, although the CD peak was slightly shifted to shorter wavelengths. This indicates that the helical structure is preserved even after iodine doping. Furthermore, CD and x-ray diffraction measurements showed that the helical structure was also preserved after heating to 150°C (which corresponds to the isomerization temperature from *cis* to *trans* form). The most stable structure of polyacetylene is the planar one. However, because the polyacetylene is insoluble and infusible, the helical structure formed during the polymerization can be preserved even if it is washed with toluene or thermally heated below the isomerization temperature. In other words, the insolubility and infusibility of polyacetylene are indispensable for preserving the metastable helical structure. Our data show that helix formation is possible not only for polyacetylene but also for π-conjugated polymers without chiroptical substituents in side chains.

Lastly, we would like to emphasize the results of the following control experiments: (i) Acetylene polymerization was carried out in a nematic LC environment using an equally weighted mixture of PCH302 and PCH304, but without the chiral dopant. The polyacetylene film showed neither helical morphology in SEM micrographs nor a Cotton effect in CD spectra. The observed morphology was composed of fibrils that were locally aligned, owing to spontaneous orientation of the LC solvent. This has also been confirmed previously (*7–9*). (ii) Next, the acetylene polymerization was performed in toluene and a small amount (less than 10%) of the chiral dopant. The synthesized polyacetylene showed the typically encountered randomly oriented fibrillar morphology, rather than the helical one. At the same time, the polyacetylene showed no Cotton effect in the CD spectrum, although the characteristic very broad absorption band due to the π → π* transitions in the conjugated polyene chain was observed in the region of from 450 to 800 nm. (iii) Acetylene polymerization at 35° to 40°C, where the LC mixture including the chiral dopant was isotropic, produced polyacetylene with no helical morphology. These results demonstrate that the chiral nematic LC environment is essential for the helical polyacetylene.

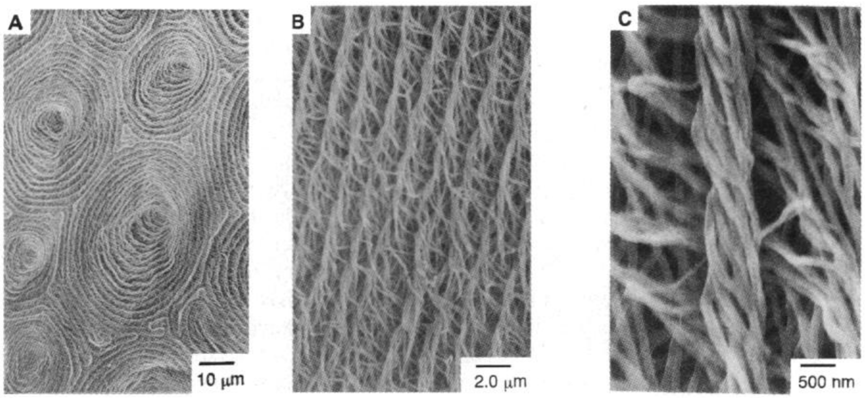

Fig. 5. SEM micrographs (at different magnifications) of helical polyacetylene films synthesized with (*R*)-chiral nematic LC including (*R*)-(+)-6,6′-bis-PCH506-2,2′-di-Et-binol as the chiral dopant (Scheme 3).

References and Notes

1. T. A. Skotheim, Ed., *Handbook of Conducting Polymers* (Dekker, New York, 1986); H. S. Nalwa, Ed., *Handbook of Organic Conductive Molecules and Polymers* (Wiley, New York, 1997).
2. H. Naarmann and N. Theophilou, *Synth. Met.* **22**, 1 (1987).
3. J. Tsukamoto, A. Takahashi, K. Kawasaki, *Jpn. J. Appl. Phys.* **29**, 125 (1990).
4. I. Božović, *Mod. Phys. Lett. B* **1**, 81 (1987).
5. H. Shirakawa and S. Ikeda, *Polym. J.* **2**, 231 (1971).
6. K. Araya, A. Mukoh, T. Narahara, H. Shirakawa, *Chem. Lett.* (no. 7), 1141 (1984); *Synth. Met.* **14**, 199 (1986).
7. K. Akagi, H. Shirakawa, K. Araya, A. Mukoh, T. Narahara, *Polym. J.* **19**, 185 (1987).
8. K. Akagi *et al.*, *Synth. Met.* **17**, 241 (1987).
9. H. Shirakawa *et al.*, *J. Macromol. Sci. Chem.* **A25**, 643 (1988).
10. K. Akagi, M. Ito, S. Katayama, H. Shirakawa, K. Araya, *Mol. Cryst. Liq. Cryst.* **172**, 115 (1989).
11. K. Akagi, S. Katayama, M. Ito, H. Shirakawa, K. Araya, *Synth. Met.* **28**, D51 (1989).
12. The difference of $[\alpha]_D$ between (*R*)- and (*S*)-binol derivatives should be ascribed to an occurrence of partial racemization during the etherification reactions between the hydroxyl groups of the binaphthols and the PCH506 substituents. Because the boiling temperature of cyclohexanone, which was used as a reaction solvent, is 157°C, it is desirable that the etherification reaction be carried out by refluxing the cyclohexanone solution around 150°C. However, to obtain a higher yield, the reaction for the (*S*)-binol derivative was refluxed at 156°C, very close to the boiling point of cyclohexanone, and for longer times (22 hours) than in the case of the (*R*)-binol derivative (150°C and 14 hours). In fact, the yield (99.6%) of the (*S*)-binol derivative was higher than that (96.9%) of the (*R*)-binol derivative. However, more racemization during the etherification reaction seems to have occurred in the (*S*)-binol derivative than in the (*R*)-binol derivative.
13. Synthesis of the (*R*)-bino derivative shown in Scheme 3. K. Akagi, S. Kaneko, G. Piao, H. Shirakawa, M. Kyotani, unpublished results.
14. It is of keen interest that the hierarchical higher order structure observed in Fig. 5 resembles the helical self-assembled microstructure of such biological molecules as lipids. See J. M. Schnur, *Science* **262**, 1669 (1993), and references therein.

15. This research was supported by Grant-in-Aids for Scientific Research from the Japanese Ministry of Education, Culture and Science, and in part by the Tsukuba Advanced Research Alliance (TARA) project of the University of Tsukuba.

30 March 1998; accepted 26 October 1998

Macroscopic Quantum Interference from Atomic Tunnel Arrays

B. P. Anderson and M. A. Kasevich

Interference of atomic de Broglie waves tunneling from a vertical array of macroscopically populated traps has been observed. The traps were located in the antinodes of an optical standing wave and were loaded from a Bose-Einstein condensate. Tunneling was induced by acceleration due to gravity, and interference was observed as a train of falling pulses of atoms. In the limit of weak atomic interactions, the pulse frequency is determined by the gravitational potential energy difference between adjacent potential wells. The effect is closely related to the ac Josephson effect observed in superconducting electronic systems.

Josephson-effect interference experiments have become paradigms for understanding the physical manifestations of the phases of macroscopic quantum systems (*1*, *2*). Bose-Einstein condensation in dilute alkali vapors (*3*) and recent interference studies with Bose-Einstein condensed atoms (*4*) raise the possibility of observing similar phase-dependent dynamics with dilute neutral-atom systems (*5*).

In the ac Josephson effect, application of a dc voltage, V, across a tunnel junction between two superconducting reservoirs leads to an alternating current through the junction with a frequency proportional to the applied voltage (*6*). The physical origin of the effect is the temporal interference of two macroscopic quantum states $|1\rangle$ and $|2\rangle$ of differing chemical potentials μ_1 and μ_2, respectively. The voltage-induced chemical potential difference between the states, $\mu_1 - \mu_2 = 2eV$, leads to a linear evolution of their relative quantum mechanical phase at a rate $(\mu_1 - \mu_2)/\hbar$ ($\hbar$ is Planck's constant, h, divided by 2π). This temporal phase slip results in an alternating current of frequency $2eV/\hbar$.

In our experiment, interference occurs between macroscopic quantum states comprising Bose-Einstein condensed atoms confined in an array of optical traps in a gravitational field. Neglecting atomic interactions, the chemical potential difference between adjacent traps is determined by the gravitational potential $U_G = mgz$, which is analogous to the applied voltage in the ac Josephson effect (m is the atomic mass, g the acceleration due to gravity, and z is the vertical coordinate). The traps are formed at the antinodes of a vertically oriented optical standing wave, which are separated by $\Delta z = \lambda/2$ (λ is the wavelength of light used to confine the atoms), and the chemical potential difference is $mg\lambda/2$. Coherent tunneling from these traps leads to a time-dependent atom current that is modulated at the frequency $\omega_J = mg\lambda/2\hbar$. This frequency depends only on fundamental constants, g, and the wavelength of the confining light.

A combined optical-plus-gravitational trapping potential similar to those used in this study is illustrated in Fig. 1. The quantum transport properties of periodic sloping potentials for single particles have been studied as models for electron motion under the influence of a static electric field in a crystal lattice (*7*). For weak external potential gradients, the external field can be treated as a perturbation to the band structure associated with the lattice. In this limit, wave packets remain confined in a single band and the external field drives coherent oscillations at the Bloch frequency (*8*). At higher field strengths, the field drives interband transitions to higher lying states, as first calculated by Zener in the context of dielectric breakdown in solids (*9*).

Our experimental parameters are in the regime where the bare lattice potential (neglecting the gravitational slope) supports only one band below its energy maximum. The width of this band is comparable to the gravitationally induced offset between adjacent wells of the combined potential. A single-particle eigenstate localizes over a small cluster of adjacent lattice sites (*10*). Particles that tunnel out of these states rapidly progress to a continuum state in which the lattice potential is a negligible perturbation on the gravitationally accelerated wave packet trajectories. The lattice states are populated in such a way that the wave function associated with the qth lattice position can be accurately described by the macroscopic state $\Psi_q = n_q^{1/2}\, e^{i\phi_q(t)}$. In the noninteracting limit, where effects due to interatomic collisions are negligible, the atom density n_q is determined by the single-particle wave function and the number of atoms, and the macroscopic phase $\phi_q(t)$ depends only on the initial phase at time $t = 0$ and the gravitational energy.

For appropriate experimental parameters, each lattice state can have a potentially significant tunneling probability into the (unbound) continuum and can be modeled as a point emitter of de Broglie waves with an emission rate proportional to the tunneling probability. The output from an array of such emitters localized at positions z_q^0 is obtained by summing over the coherent emission from each well. For an array of N traps the emission is

$$\Psi(z,t) = \sum_{q=1}^{N} A_q(t)\exp\left[\, i\int (k_q dz - \omega_q dt + \phi_q^0)\right] \tag{1}$$

where $\hbar k_q = m\sqrt{2g|z - z_q^0|}$ and $\hbar\omega_q =$

Physics Department, Yale University, New Haven, CT 06520, USA.